DOI 10.1007/s11141-023-10279-3
Radiophysics and Quantum Electronics, Vol. 66, Nos. 2–3, July–August, 2023
(Russian Original Vol. 66, Nos. 2–3, February–March, 2023)

ON THE INFLUENCE OF MICROBUBBLES ON THE TURBULENCE INDUCED BY A SURFACE WAVE

O. A. Druzhinin*

UDC 551.465

We use the direct numerical simulation (DNS) method to study the vortex structure of the near-surface water layer, which is saturated with air bubbles, in the presence of a stationary surface wave. A wave with a wavelength of 15 *cm and a steepness of* 0.2 *(an amplitude of about* 0.5 *cm) and bubbles* 400 *μm in diameter (microbubbles) are considered. Complete three-dimensional fluid motion equations (Navier–Stokes equations) are solved by the DNS method simultaneously with the equations of motion of individual bubbles with allowance for their influence on the carrier flow. Under the influence of the surface wave, the flow in the near-surface layer becomes turbulent and characterized by the presence of vortex structures stretched along the wave propagation direction. To analyze the vortex structure of the flow, the instantaneous velocity gradient tensor is calculated, and its complex eigenvalues, whose imaginary part characterizes the local vorticity of the flow, are calculated, while filtering out the contribution of the purely shear component (vortex sheet). Average profiles of the eigenvalues and the fluctuations, which are obtained at the stage of the statistically stationary flow, show that the influence of the bubbles lead to intensification of small-scale vortices and turbulent pulsations in water.*

1. INTRODUCTION

Small-scale processes occurring near a water surface play the determining part in the exchange of the momentum, heat, and moisture between the atmosphere and the hydrosphere. Thorough understanding of the physical mechanisms of these processes is of utmost importance for their accurate parametrization in large-scale prognostic models [1, 2]. The presence of air (gas) bubbles in the near-surface water layer is one of the many factors which should be allowed for when developing the exchange models.

Breaking (or microbreaking) of surface waves is one of major sources of air bubbles in the near-surface water layer [3, 4]. Another source of gas bubbles, which has intensely been studied recently, is the bottom release of methane (see, e.g., [5]). The observations in laboratory and full-scale experiments [3, 6–8], as well as in the numerical experiment [9], show that bubbles about hundreds of micrometers in diameter (microbubbles) make the main contribution to the volumetric fraction of the air phase and the typical distribution with respect to the diameters of the suspended bubbles. According to the data of full-scale observations, the volumetric fraction of microbubbles in the top layer of the ocean can reach significant values (about 10^{-5}) even in a relatively weak wind (about several meters per second) [10–14]. Therefore, studying and modeling of the dispersion of microbubbles, as well as assessing of their influence on small-scale turbulence in the near-surface layer of the hydrosphere are rather important issues.

The influence of bubbles on the near-surface turbulence was studied using the direct numerical simulation (DNS) method in [15, 16]. Complete three-dimensional equations of fluid motion (Navier–Stokes

* druzhinin@ipfran.ru

Institute of Applied Physics of the Russian Academy of Sciences, Nizhny Novgorod, Russia. Translated from Izvestiya Vysshikh Uchebnykh Zavedenii, Radiofizika, Vol. 66, Nos. 2–3, pp. 122–129, February–March 2023. Russian DOI: 10.52452/00213462_2023_66_02_122 Original article submitted January 23, 2023; accepted March 31, 2023.

equations) were solved within the Eulerian formulation simultaneously with the Lagrangian equations of the bubble motion with allowance for their influence on the carrier phase. Within the DNS method, the bubble diameters were specified in the range from 200 μm to 400 μm, which allowed us to neglect deformations of the bubbles. The results of these calculations show that the main part in the bubble dynamics is played by the forces of buoyancy, viscous friction, and Lagrangian acceleration, whereas the lift force, which is determined by the vorticity of the carrier phase and the relative bubble velocity, remains negligibly small. It is also shown that the horizontal transfer of the bubbles is controlled by the velocity of the Stokes drift, whereas the vertical flow is determined by the velocity of up-floating of the bubbles in water at rest. Based on the data obtained in [15, 16], parametrizations of the vertical and horizontal flows of the volumetric fraction of the air phase in the near-surface water layer were proposed. However, the influence of the bubbles on vortex structures has not been studied thoroughly yet.

The purpose of this work is to study the influence of the bubbles on vortex structures and the turbulence induced by a non-breaking surface wave. We use the algorithms developed in [15, 16] to calculate the dynamics of the water environment bounded by a wavy surface (including allowance for the surface drift induced by the shear wind stress) and saturated with air microbubbles. In order to evaluate quantitatively the influence of the bubbles on the dynamics of coherent vortex structures, we apply the algorithm used to calculate the field of eigenvalues of the instantaneous velocity gradient tensor in the air boundary layer [17]. Section 2 describes briefly the DNS procedure and presents the technique of statistical processing of the results and the method used to calculate the eigenvalues of the instantaneous velocity gradient tensor. Section 3 describes and analyzes the calculation results. The conclusions are drawn in Sec. 4.

2. MATHEMATICAL MODEL

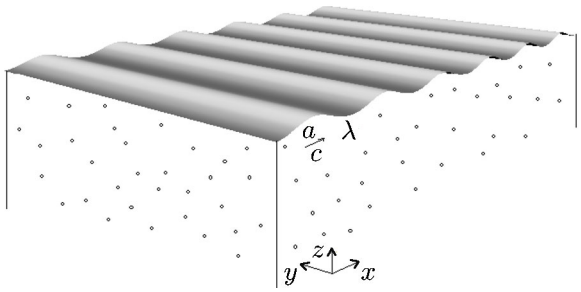

Fig. 1. Scheme of the numerical experiment.

The general scheme of the numerical experiment is shown in Fig. 1.

We consider an infinitely deep calculation area with the upper boundary coinciding with the water surface. A two-dimensional stationary wave having the amplitude a, the wavelength λ (wave number $k = 2\pi/\lambda$), and the wave steepness $ka = 2\pi a/\lambda$ propagates along this surface. The values $\lambda = 15$ cm and $ka = 0.2$ (the amplitude $a \approx 0.5$ cm) are specified within the DNS method. For the specified wavelength, the phase velocity determined by the linear dispersion relation [1] is $c \approx 49$ cm/s. Thus, the Reynolds number determined by c and λ is Re ≈ 73019. In what follows, we consider the dimensionless variables normalized to c and λ. At each time instant t under consideration, the DNS method uses a conformal map of the Cartesian coordinates in the vertical plane, which converts an infinitely deep area with the wave-shaped upper boundary into an area bounded by the upper and lower plane boundaries (at $\eta = 0$ and -1). In this case, the shape of the water surface is specified implicitly and coincides with the solution for the Stokes wave with accuracy up to the second-order infinitesimal terms with respect to ka [15]. All the fields are periodic with respect to the horizontal coordinates. On the water surface, the conditions for the water velocity are specified in accordance with the potential solution for the surface wave, both with and without allowance for the wind surface drift. The known parametrization is used for the velocity of the surface drift in terms of the parameters of the surface wave [1, 18]. At the lower boundary, the condition of the absence of normal gradients (the Neumann condition) is specified.

The system of Navier–Stokes equations for water is solved numerically in the Eulerian formulation simultaneously with the equations for the Lagrangian dynamics of individual bubbles with allowance for the phase interaction (see a more detailed discussion of the DNS procedure in, e.g., [15]). At the initial stage of the calculations, a random three-dimensional field of the water velocity is specified with a small amplitude (about 0.1% of the amplitude of the wave velocity field). At the upper boundary, at each time instant a

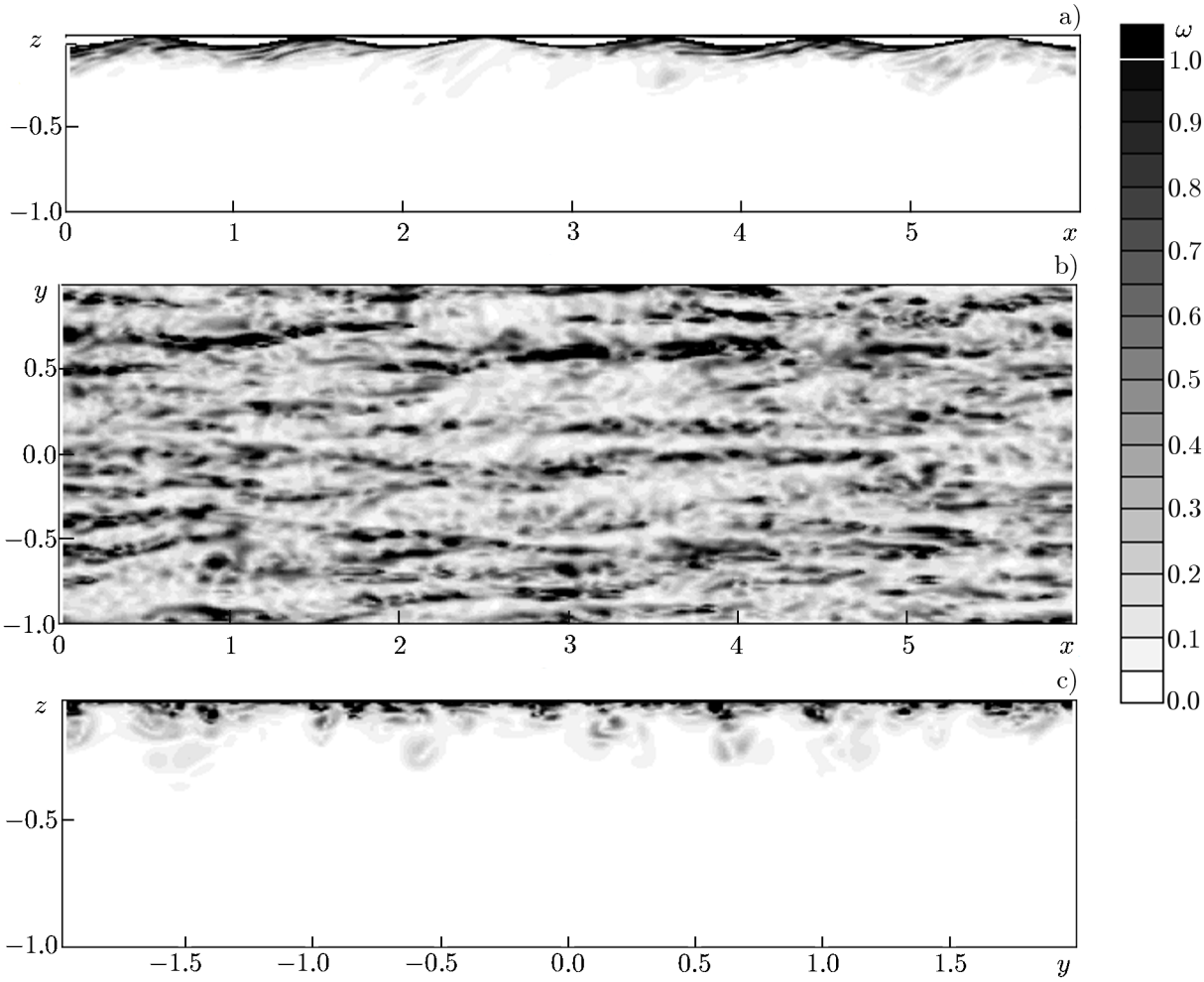

Fig. 2. Instantaneous vorticity modulus field in the presence of a surface drift flow without bubbles in different planes: side view ($y = 0$) (*a*), top view ($\eta = -0.05$) (*b*), and profile ($x = 3$) (*c*).

two-dimensional velocity field is specified, which is determined by the potential solution of the second-order accuracy for the Stokes wave on deep water [1]. The bubbles are injected randomly in the bulk of water with spatial probability distribution, which decreases exponentially with increasing depth, and the velocity equal to the instantaneous velocity of the water environment. The bubbles that reach the surface are reinjected, so that the total number of bubbles is kept constant during the entire duration of the calculations.

To estimate quantitatively the influence of bubbles on the dynamics of coherent vortex structures, we use an algorithm for calculating the field of eigenvalues of the instantaneous velocity gradient tensor [18, 19]. The squared imaginary part of the complex eigenvalues is determined by the formula

$$\gamma_c^2 = \frac{3}{4}\left[(R + P^{1/2})^{1/3} - (R - P^{1/2})^{1/3}\right]^2, \tag{1}$$

where

$$R = \frac{1}{2}\det\left\|\frac{\partial \hat{U}_i}{\partial x_j}\right\|, \qquad P = \frac{Q^3}{27} + R^2, \qquad Q = -\frac{1}{2}\mathrm{tr}\left\|\frac{\partial \hat{U}_i}{\partial x_j}\right\|^2, \tag{2}$$

and $\hat{U}_i$ ($i = x, y, z$) is the water velocity field minus the phase-averaged component [17]. The phase-averaged flow fields are determined, as the stationary regime becomes stable (at times of about 200 wave periods), by the averaging with respect to the time and the transverse coordinate, as well as the "window" averaging with respect to the wave phase. The time averaging is performed over instantaneous fields at sequential

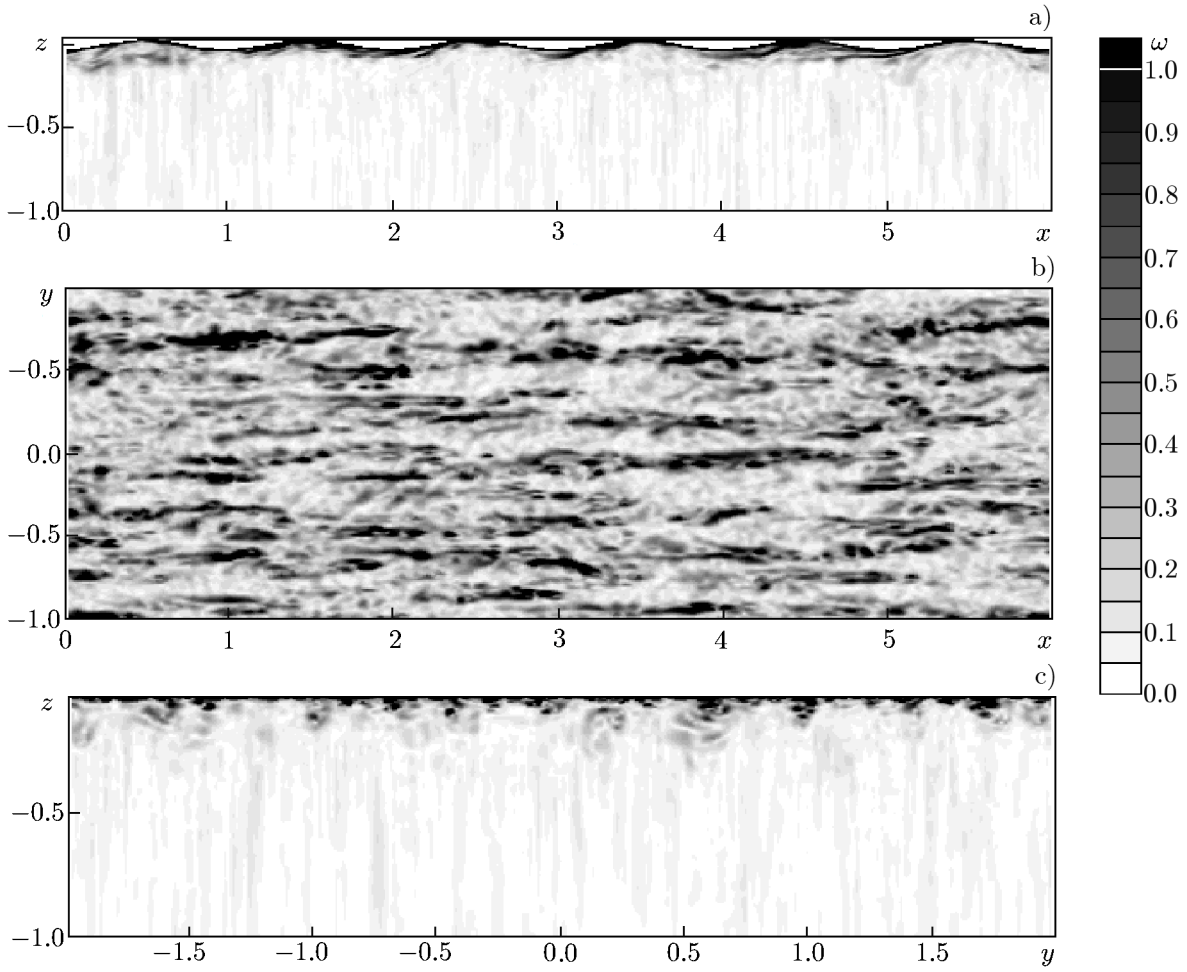

Fig. 3. Same as in Fig. 2 but in the presence of the bubbles.

time instants, at which the surface-wave phase differs by 2π. The vertical profiles are determined by the additional averaging of the field with respect to the wavelength.

3. MODIFICATION OF THE WAVE-INDUCED TURBULENCE BY BUBBLES

The DNS calculations were performed for one given wavelength (λ = 15 cm) and the steepness $ka = 0.2$ of the surface wave for the single- and double-phase cases, both in the presence and absence of the surface drift. We considered a monodispersed suspension of bubbles 400 μm in diameter, whose total number was maintained at a constant level ($N_{\rm d} = 1.26 \cdot 10^5$).

Figures 2 and 3 present the instantaneous fields of the vorticity modulus ω, which is determined according to the equalities

$$\omega = (\omega_i \omega_i)^{1/2}, \ \omega_i = \varepsilon_{ijk} \partial U_i / \partial x_j, \ i, j = x, y, z, \tag{3}$$

where ε_{ijk} is the Levi–Civita symbol, at the stage of the statistically stationary flow in the presence of the surface drift in the single- and double-phase cases, respectively. In the absence of the surface drift, the vorticity fields look similar qualitatively. It is seen in the figures that in both cases, the flow is characterized by the presence of vortex structures stretched along the propagation direction of the surface wave. This flow pattern agrees qualitatively with the results of the numerical experiment [20], in which similar vortex structures were also observed in the surface-wave field. Figure 3 also shows that up-floating bubbles produce disturbances in the form of vortex structures stretched vertically. The corresponding trajectories of individual bubbles are shown in Fig. 4.

For all the cases under consideration (single- or two-phase and with or without the drift flow), we calculated the average profiles of r.m.s. fluctuations of the velocity components:

$$U_i' = [U_i^2] - [U_i]^2, \qquad i = x, y, z, \tag{4}$$

and the squared imaginary part $[\gamma_c^2]$ of the complex eigenvalues of the velocity gradient tensor of water, where the square brackets denote averaging with respect to the horizontal coordinates and the time. Then, we calculated the relative variations in these quantities, which were affected by the air phase, according to the expressions

$$\Delta U_i' = \frac{U_{i,2w}' - U_{i,1w}'}{\max\{U_{i,1w}'\}}, \qquad \Delta\gamma = \frac{[\gamma_c^2]_{2w} - [\gamma_c^2]_{1w}}{\max\{[\gamma_c^2]_{1w}\}}, \tag{5}$$

where the subscripts 1w and 2w correspond to the single- and two-phase flows, respectively. Figure 5 shows the vertical profiles (5) obtained in the absence and presence of the drift flow.

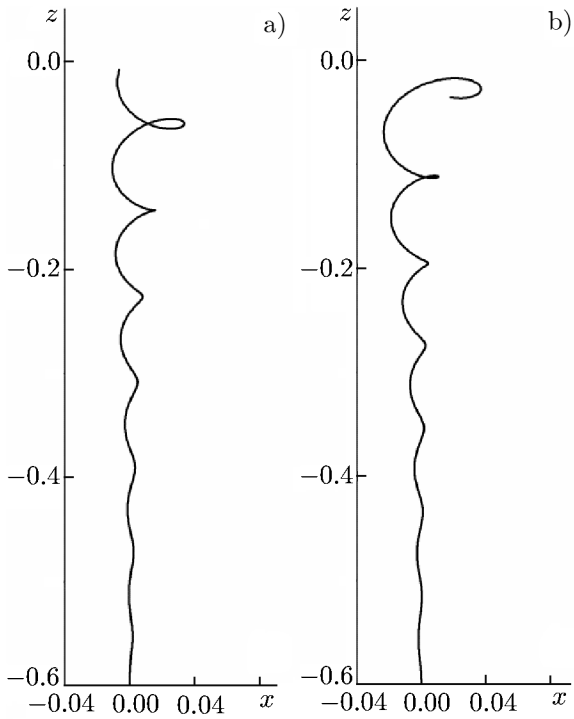

Fig. 4. Trajectories of individual bubbles in the absence (*a*) and presence (*b*) of the surface drift.

One can see in Fig. 5 that in both cases (i.e., in the absence and presence of the surface drift), the vertical component of the water velocity having the maximum $\Delta U_z' \approx 1.7$ at the depth of about the wavelength of the surface wave experiences the maximum relative change. However, the maximum variation takes place in the vertical velocity component sufficiently close to the surface, at the depth of about 0.01λ, ($\Delta U_z' \approx 0.8$ in the absence of the drift and $\Delta U_z' \approx 1.3$ in the presence of the surface drift). At the same depth, the maximum value of $\Delta\gamma$ is observed (about 0.2 in the absence of the drift and 0.8 in the presence of the surface drift).

The data for the modification of the turbulence in Fig. 5 agree qualitatively with instantaneous distributions of the vorticity and bubble trajectories (see Figs. 3 and 4). One can see in these figures that the bubble trajectories are almost rectilinear at a sufficient distance from the surface, since the influence of wave motions and the near-surface turbulence that they induce is exponentially small here. Therefore, the main influence of the air phase in this region mainly influences the vertical component of the water velocity, which leads to an increase in the fluctuation of this component (see Fig. 5). As the bubbles approach the surface, their trajectories take the form of unwinding helices. This leads to an increase in their influence on the other components of the water velocity, which results in stronger fluctuations and vortivity of the local turbulent vortices (qualitatively, it is manifested in the modification of dispersion of $\Delta U_i'$ and $\Delta\gamma$; see Fig. 5).

4. CONCLUSIONS

Direct numerical simulation of the near-surface water layer saturated with air bubbles in the presence of a stationary surface wave has been performed. Complete three-dimensional water motion equations (Navier–Stokes equations) are solved within the Eulerian formulation simultaneously with the Lagrangian motion equations of the bubbles with allowance for their influence on the carrier phase.

The results show that under the influence of the surface wave, the flow in the near-surface layer becomes turbulent and is characterized by the presence of vortex structures stretched along the wave propagation direction. In order to analyze the vortex structure of the flow, the instantaneous velocity gradient tensor is calculated and its complex eigenvalues are determined. The imaginary part of the eigenvalues characterizes local vorticity of the flow, filtering out the contribution of the purely shear component (the vortex sheet). The average profiles of the eigenvalues and fluctuations, which are obtained at the stage of the

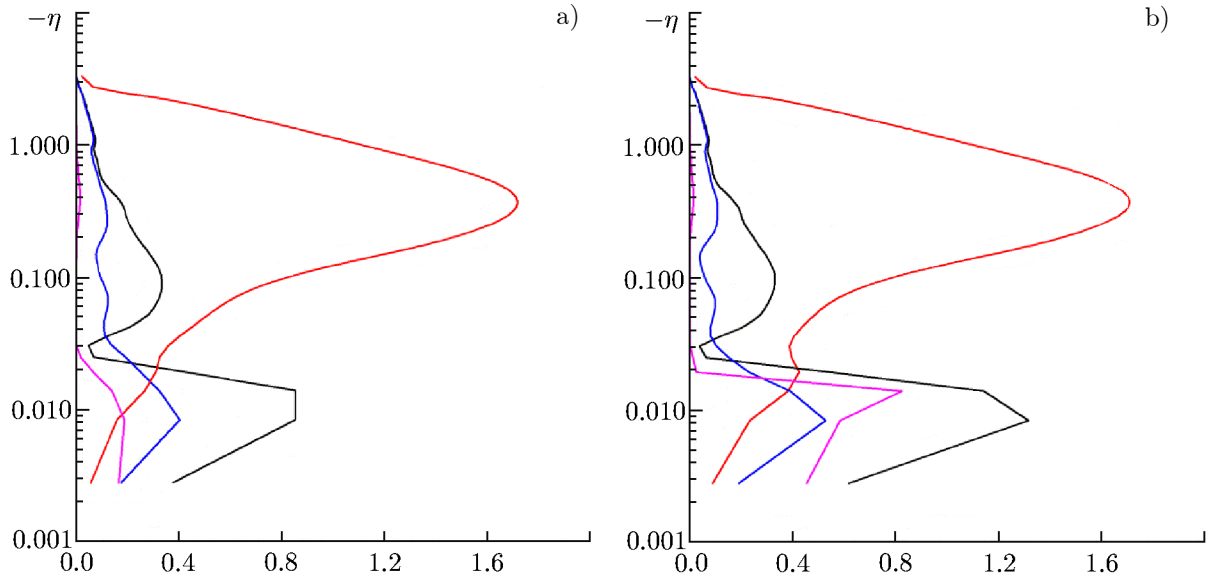

Fig. 5. Vertical profiles of the differences $\Delta U_i'$ of the r.m.s. fluctuations (black, blue, and red lines refer to $i = x$, y, and z, respectively) and the differences $\Delta\gamma$ (violet lines) of the squared imaginary part of eigenvalues of the water velocity gradient tensor, calculated according to Eq. (5) in the double- and single-phase cases in the absence (*a*) and presence (*b*) of the surface drift.)

statistically stationary flow, show that under the influence of the bubbles, small-scale vortices and turbulent pulsations in water become stronger.

It should be noted that the surface wave is assumed given in this work. The self-consistent problem with allowance for the modification of the surface wave by the near-surface turbulence and bubbles remains to be considered in future studies.

The development of the numerical algorithms, as well as the processing and theoretical analysis of the results obtained were supported by the Russian Foundation for Basic Research (project No. 21–55–52005). The computer calculations were performed on the computing cluster of the Institute of Applied Physics (state assignment No. 0030–2022–0005).

REFERENCES

1. O. M. Phillips, *The Dynamics of the Upper Ocean*, Cambridge Univ. Press, Cambridge (1980).
2. S. A. Thorpe, *Prog. Oceanogr.*, **35**, 315–352 (1995). https://doi.org/10.1016/0079-6611(95)80002-B
3. P. A. Kolovaev, *Oceanology*, **15**, 659–661 (1976).
4. B. D. Johnson and R. C. Cooke, *J. Geophys. Res.*, **84**, 3761–3766 (1979). https://doi.org/10.1029/JC084iC07p03761
5. J. Steinbach, H. Holmstrand, K. Shcherbakova, et al., *Proc. Natl. Acad. Sci. U.S.A.*, **118**, No. 223, Art. no. e2019672118 (2021). https://doi.org/10.1073/pnas.2019672118
6. H. Medwin, *J. Geophys. Res.*, **82**, 971–976 (1977). https://doi.org/10.1029/JC082i006p00971
7. G. B. Dean and M. D. Stokes, *Nature*, **418**, 839–844 (2002). https://doi.org/10.1038/nature00967
8. C. E. Blenkinsopp and J. R. Chaplin, *Proc. Roy. Soc. Lond. A*, **463**, 3151–3170 (2007). https://doi.org/10.1098/rspa.2007.1901
9. L. Deike, W. K. Melville, and S. Popinet, *J. Fluid Mech.*, **801**, 91–129 (2016). https://doi.org/10.1017/jfm.2016.372

10. D. K. Woolf and S. A. Thorpe, *J. Mar. Res.*, **49**, 435–466 (1991).
11. L. Merlivat and L. Memery, *J. Geophys. Res.*, **88**, 707–724 (1983). https://doi.org/10.1029/JC088iC01p00707
12. D. C. Blanchard, *Estuaries*, **12**, 127–137 (1989). https://doi.org/10.2307/1351816
13. D. M. Farmer and D. D. Lemon, *J. Phys. Oceanogr.*, **14**, 1762–1778 (1984). https://doi.org/10.1175/1520-0485(1984)014<1762:TIOBOA>2.0.CO;2
14. M. J. Buckingham, *Appl. Acoust.*, **51**, 225–250 (1997). https://doi.org/10.1016/S0003-682X(97)00002-9
15. O. A. Druzhinin and W.-T. Tsai, *Algorithms*, **15**, 110 (2022). https://doi.org/10.3390/a15040110
16. O. A. Druzhinin, *Izv. Atmos. Ocean. Phys.*, **58**, No. 5, 507–515 (2022). https://doi.org/10.1134/S0001433822050024
17. O. A. Druzhinin and W.-T. Tsai, *J. Mar. Sci. Eng.*, **10**, 856 (2022). https://doi.org/10.3390/jmse10070856
18. D. Yang and L. Shen *J. Fluid Mech.*, **650**, 131–180 (2010). https://doi.org/10.1017/S0022112009993557
19. J. Zhou, R. J. Adrian, S. Balachandar, and T. M. Kendall, *J. Fluid Mech.*, **387**, 353–240 (1999). https://doi.org/10.1017/S002211209900467X
20. W.-T. Tsai, S.-M. Chen, and G.-H. Lu, *J. Phys. Oceanogr.*, **45**, 174–180 (2015). https://doi.org/10.1175/JPO-D-14-0121.1